Experimental Mechanics (2006) 46: 269–281
DOI 10.1007/s11340-006-5863-4

Mixed-Mode Dynamic Crack Growth in Functionally Graded Glass-Filled Epoxy

M.S. Kirugulige · H.V. Tippur

Received: 18 August 2005 / Accepted: 13 October 2005 / Published online: 17 February 2006

Abstract Compositionally graded glass-filled epoxy sheets with edge cracks initially along the gradient are studied under dynamic loading conditions. Specimens with monotonically varying volume fraction of reinforcement are subjected to mixed-mode loading by eccentric impact relative to the crack plane. The optical method of Coherent Gradient Sensing and high-speed photography are used to map transient crack tip deformations before and after crack initiation. Two configurations, one with a crack on the stiffer side of a graded sheet and the second with a crack on the compliant side, are examined experimentally. To elucidate the differences in fracture behavior due to functional grading, a homogeneous sample is also tested. The differences in both pre- and post-crack initiation behaviors are observed in terms of crack initiation time, crack path, crack speed and stress intensity factor histories. When a crack is situated on the compliant side of the sample, it kinks significantly less compared to when it is on the stiffer side. Crack tip mode mixity histories show small but positive values during crack growth from the stiffer side of the sample towards the compliant side whereas a small but negative mode mixity prevails for the opposite configuration.

Keywords Dynamic fracture · Functionally graded materials · Coherent Gradient Sensing · Mixed-mode fracture · Crack path selection

M.S. Kirugulige (SEM member) · H.V. Tippur (✉, SEM member)
Department of Mechanical Engineering,
Auburn University, Alabama 36849, USA
e-mail: htippur@eng.auburn.edu

Introduction

Functionally graded materials (FGM) are generally two-phase composites with continuously varying volume fraction of the constituents. They are used in various applications—as thermal barrier coatings in high temperature components, as inter layers in micro-electronic packages, as core material in impact resistant sandwich structures, etc.—to name a few. FGM are macroscopically nonhomogeneous regarding mechanical properties such as elastic modulus, mass density, strength and fracture toughness. The knowledge of crack propagation in the presence of compositional gradients is essential in order to evaluate their mechanical integrity. The role of spatial grading on fracture behavior under mixed-mode loading conditions is studied in this work experimentally.

The stress intensity factors in FGM are affected by compositional gradients even though the inverse $\sqrt{r}$ singularity near the crack tip is preserved [1, 2]. Issues pertaining to the fracture mechanics of FGM under static loading have been addressed in the recent literature. Jin and Batra [3], Gu and Asaro [4] provide quasi-static stress intensity factors for cracks in FGM for different geometry and loading conditions. Shukla and coworkers [5, 6] have reported crack tip stress fields for dynamically growing cracks in functionally graded materials for mode-I and mixed-mode loading conditions. They have derived asymptotic expressions for stresses and displacements in FGM with linear and exponential variations of elastic modulus. Tippur and his coworkers [7–10] have addressed several issues related to mode-I dynamic fracture of FGM. Among numerical studies related to FGM, Wang and Nakamura [11] have simulated crack propagation in elastic-

plastic graded materials using cohesive elements. Kim and Paulino [12] have addressed issues pertaining to crack path trajectories in FGM under mixed-mode and non-proportional loading conditions.

When a crack in FGM is not parallel to the direction of material property variation or loading is asymmetric relative to the crack plane or both, fracture is inherently mixed-mode in nature. These introduce both normal and shear tractions ahead of the crack tip. Therefore mixed-mode crack propagation in FGM needs to be studied in order to characterize fracture behavior under such circumstances. To date, very few studies have been reported in the literature about experimental investigation of mixed-mode fracture in FGM. Instead, most reported works deal with mixed-mode fracture of homogeneous materials or bi-layered materials. For example, Ramaswamy et al. [13] have successfully used Coherent Gradient Sensing (CGS) to study mixed-mode crack tip deformations under static loading using a modified flexural specimen geometry. Situation involving a crack located in a homogeneous material but close to an interface between two dissimilar linear elastic materials is examined by Lee and Krishnaswamy [14]. Mason et al. [15] have used CGS to map mode-I and mode-II stress intensity factors in homogeneous polymer sheets under dynamic loading conditions. Prabhu and Lambros [16] have studied mode-I and mixed-mode crack tip fields in homogeneous materials using combined methods of CGS and caustics. Madhusudhana and Narasimhan [17] have studied crack growth resistance of ductile adhesive joints under mixed-mode, quasi-static loading conditions using modified compact tension-shear specimen. Among the experimental investigations on mixed-mode fracture of FGM, works of Butcher et al. [18], Rousseau and Tippur [19] and Marur and Tippur [20] are noteworthy. In Ref. [18], feasibility of processing glass-filled epoxy beams for mixed-mode static fracture studies using optical interferometry has been demonstrated. The role of material gradation on crack kinking under static loading conditions has been studied in Ref. [19]. The possibility of using optimally positioned strain-gages near a crack tip undergoing mixed-mode loading to obtain SIF histories during impact loading has been demonstrated in Ref. [20].

Evidently, at the moment experimental studies on mixed-mode fracture of FGM are largely absent in the literature. The aim of the present investigation is to study the role of functional grading on crack path during a mixed-mode dynamic fracture event. Compositionally graded glass-filled epoxy sheets with initial cracks along the gradient and subjected to one point impact are studied. Initial mode mixity is generated by impacting the sample eccentrically relative to the crack plane. The optical method of CGS along with high-speed photography is used to map transient crack tip deformations before and after crack initiation. Two configurations are studied experimentally. In the first one, an edge crack is located on the stiffer side of the sample while impact occurs on the compliant side where as in the second the crack is on the compliant side with impact occurring on the stiffer side. A homogeneous specimen with similar dimensions as FGM samples is also studied for comparison.

Material Processing and Characterization

FGM samples were prepared by continuously varying the volume fraction of filler particles in the matrix. Solid soda-lime spherical glass particles (Spheriglass #3000, 35 μm diameter, uncoated, from Potters Industries, Inc., USA) were used as the filler material. A low-viscosity, room temperature curing epoxy prepared by mixing bisphenol-A resin and amine based hardener in the ratio 100:36 was used as the matrix material. Bulk elastic properties of the filler and the matrix are listed in Table 1.

The material preparation consisted of mixing 40% volume fraction of glass particles into the epoxy resin. Sufficient care was exercised in order to avoid entrapment of air bubbles. The time period between mixing of particles and pouring into the mold was optimized to get a compositional gradient over the desired height of the sample. The gravity assisted casting method used here produced a nearly linear variation of volume fraction of glass particles in the vertical direction. The details are avoided here for brevity and can be found in Butcher et al. [18]. Once the specimens were cured, they were removed from the mold and rested for a week before machining to the dimensions shown in Fig. 1. A grayscale is used to schematically represent the compositional gradation (i.e., the mass density is maximum at the bottom of the sample and decreases with height). Ultrasonic pulse-echo technique was used to measure material properties. A longitudinal wave transducer (Panametrics #V129RM; 10 MHz, dia = 5 mm) and a shear wave

Table 1 Nominal bulk properties of the constituent materials

	E (GPa)	ν	ρ (kg/m^3)
Epoxy	3.2*	0.34*	1175
Soda-lime Glass**	70.0	0.23	2500

* Static data, ** Potters industries, Inc

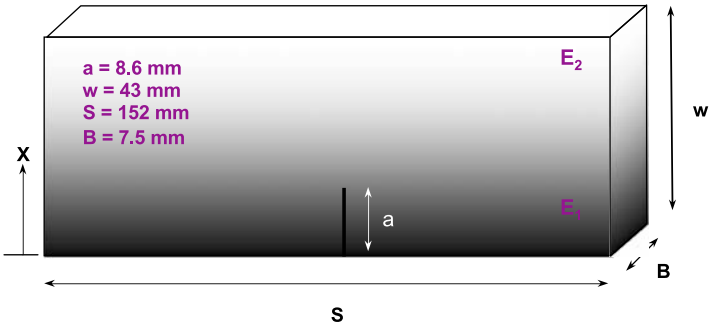

Fig. 1. Schematic of FGM sample used in experiments

transducer (Panametrics #V156RM; 5 MHz, dia = 7 mm) were used to measure wave speeds C_L and C_S respectively, at discrete locations in the sample. The variations of C_L and C_S along the width of the sample are shown in Fig. 2. A look-up chart of mass density ρ as a function of longitudinal wave speed C_L is available for glass-filled epoxy in Ref. [18]. By using measured values of C_L and C_S and the value of ρ from calibration curves, elastic moduli and Poisson's ratios were estimated along the width of the sample using,

$$C_L = \sqrt{\frac{E(1-\upsilon)}{\rho(1+\upsilon)(1-2\upsilon)}},\ C_S = \sqrt{\frac{E}{2\rho(1+\upsilon)}}. \qquad (1)$$

Elastic modulus and mass density variations along the width of the machined sample are shown in Fig. 3. It can be seen from this figure that the elastic modulus varies in a sigmoidal fashion from ~10 GPa to ~4 GPa over a width of 43 mm. The mass density varies from ~1750 kg/m^3 to ~1200 kg/m^3 over the same width. The corresponding Poisson's ratio variation was between 0.33 and 0.37. This variation in υ was not expected to play a significant role in the fracture behavior of FGM [2]. Therefore a constant value of υ = 0.34 was chosen throughout this work.

Mode-I crack initiation toughness tests were also conducted on homogeneous samples of various volume fractions (0%, 7%, 14%, 21%, 28% and 35%) of the filler. Beam samples of dimensions 152 mm × 43 mm and 7.5 mm were machined for fracture tests. An edge crack of length 10 mm (a/W = 0.23) was cut along the mid-span in each of these samples. The so-called Dally-Sanford single strain gage method [21] was used to obtain dynamic stress intensity factor histories. A strain gage of gage length 0.8 mm (CEA-13-032WT-120 from Vishay-Micromeasurements Group, Inc.) was located at a radial distance of 5.5 mm from the crack tip and at an angle of 60° to the crack orientation. These specimens were impact loaded (impact velocity ~4.5 m/sec) in 3-point bend configurations using Instron 9250-HV drop-tower. The strain history recorded was used to obtain crack initiation toughness values as detailed in Ref. [22]. Figure 4 shows the variation of mode-I crack initiation toughness (K_{ICR}) with Young's modulus. An approximately monotonic increase in the crack initiation toughness values can be seen at lower volume fractions (and lower values of E). Increase in fracture toughness by a factor of 1.5 is evident when glass filler volume fraction increases from 0 to 35% with a corresponding change in Young's modulus by a factor of 2.4.

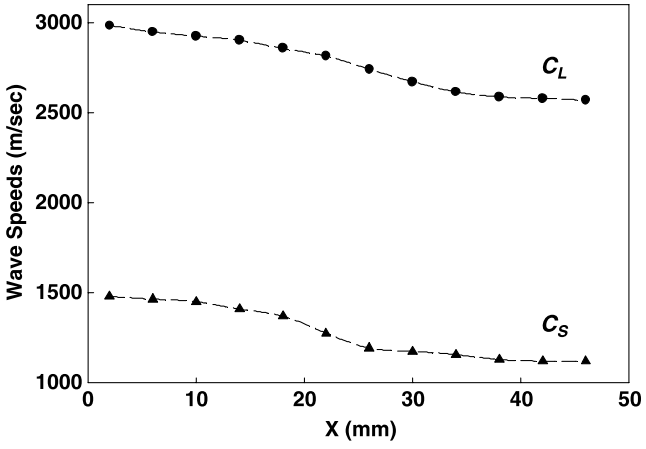

Fig. 2. Variation of longitudinal and shear wave speeds along the width of the sample

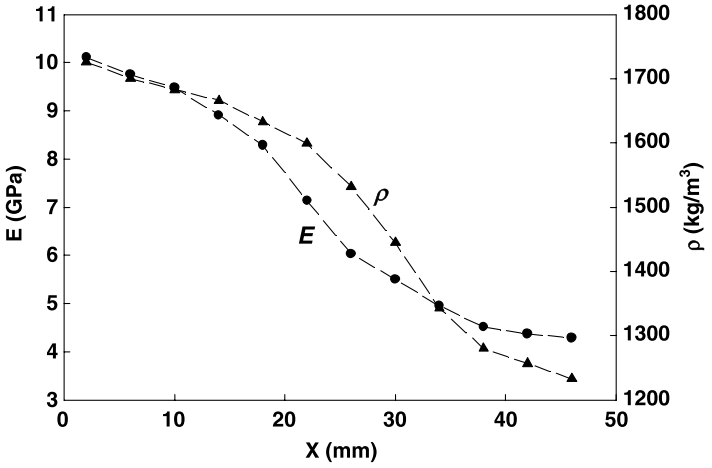

Fig. 3. Variation of elastic modulus and mass density along the width of the sample

Next, the specimens were prepared for optical tests. The specimen surface was roughened by #400 grit sandpaper. The region around the crack tip was made optically flat and specular by transferring a thin layer of aluminum (~100 nm thick) coated on an optically flat glass disc using a layer of epoxy (~10 μm thick). An edge crack (root radius ~150 μm) of length 8.6 mm (a/W = 0.2) was cut into the sample using a high-speed diamond impregnated circular saw.

Experimental Set-Up

Coherent Gradient Sensing [23] in conjunction with high-speed photography was used in this study to perform real-time measurement of instantaneous surface deformations around the crack tip. CGS measures in-plane gradients of out-of-plane surface displacements (surface slopes) around a crack tip when used to study opaque solids. A schematic of the optical set-up is shown in Fig. 5. The measurement system consisted of an impactor, pulse-laser, CGS interferometer and a continuous access high-speed camera. The specimen was initially rested on two blocks of soft putty to preclude any interaction from the supports while the specimen undergoes stress wave loading. An argon-ion laser beam (wavelength λ = 514 nm) was expanded and collimated into a 50 mm diameter beam. During the experiment, a pneumatically operated impactor-head was launched towards the specimen (speed ~5.2 m/s). During its descent, it first triggered a photo-detector to open a capping shutter located in front of the high-speed camera, allowing light to reach its internal cavity. When the impactor-head contacted the specimen, it closed an electrical circuit initiating a series of laser pulses for a duration corresponding to a single sweep of the laser beam on a stationary film track. The light entering the camera was reflected-off of a spinning three-facet mirror mounted on a turbine shaft. The reflected light beam was swept on the film held in a track as discrete images. At the end of that period, the capping shutter was closed to prevent overwriting on the film. In the current experiments, the

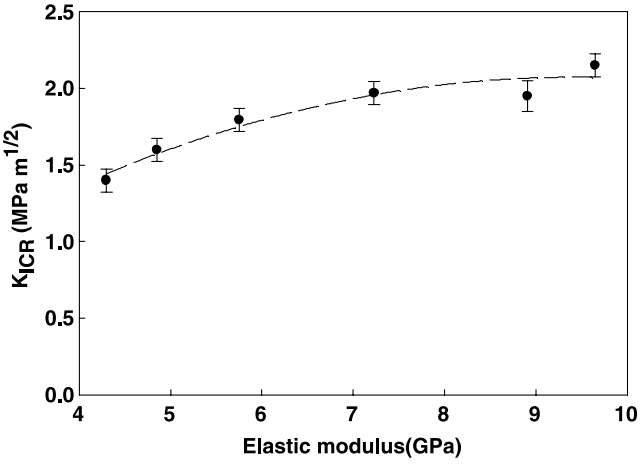

Fig. 4. Variation of dynamic initiation toughness (impact velocity = 4.5 m/sec) with Young's modulus. (Broken line is a trend line)

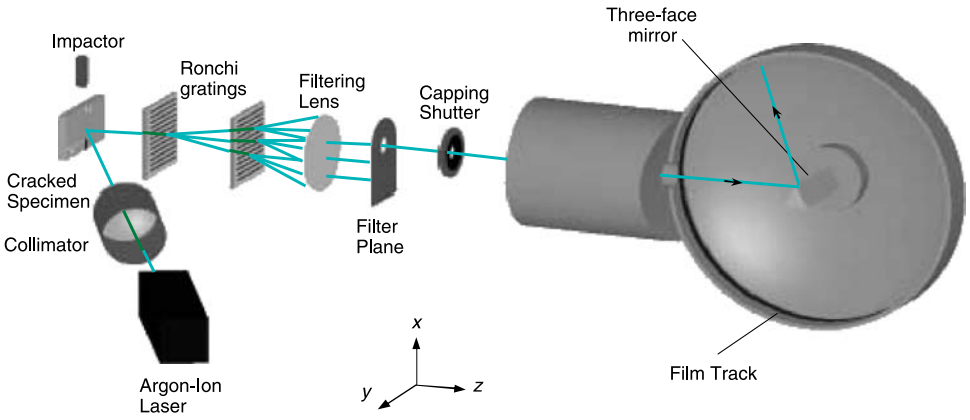

Fig. 5. Schematic for reflection mode CGS and high-speed photography

laser pulse was repeated every 5 μs (200,000 frames per second) with a pulse width of 40 ns and a total recording duration of approximately 320 μs.

The reflected light beam off the specimen surface carries information about local surface deformations. The light beam was processed using CGS interferometer comprising of a pair of Ronchi gratings (chrome-on-glass gratings) and a Fourier filtering/imaging lens. The resulting fringes represent surface slopes in the initial crack direction. Using governing equations of reflection mode-CGS and plane stress approximation, optical measurements can be related to deformations using,

$$\frac{\partial \mathrm{w}}{\partial \mathrm{X}_1} \approx \frac{\partial}{\partial \mathrm{X}_1}\left(\frac{-\upsilon B}{2E}\left(\sigma_x+\sigma_y\right)\right)=\frac{Mp}{2\Delta} \tag{2}$$

where M (=0, ±1, ±2, ...) denotes fringe order, p is the pitch of the gratings (25 μm), Δ is the grating separation distance (49 mm), B is the specimen thickness. Here X_1 is the principal direction of the gratings oriented in the same direction of the initial crack.

Fringe Analysis: Extraction of K_I and K_{II}

By expressing $\sigma_x + \sigma_y$ in equation (2) using asymptotic expansion, in-plane gradients of out-of-plane displacement become [23, 24]:

$$\frac{\partial w(t)}{\partial X_1}=-\frac{\upsilon B}{2E}\left[\sum_{N=1}^{\infty} C_N(t)\left(\frac{N}{2}-1\right) r^{\left(\frac{N}{2}-2\right)}\cos\left[\left(\frac{N}{2}-2\right)\theta\right]\right] =\frac{Mp}{2\Delta}, \tag{3}$$

$$\frac{\partial w(t)}{\partial X_2}=-\frac{\upsilon B}{2E}\left[\sum_{N=1}^{\infty} \mathrm{C}_N(t)\left(\frac{N}{2}-1\right) r^{\left(\frac{N}{2}-2\right)}\sin\left[\left(\frac{N}{2}-2\right)\theta\right]\right] =\frac{Mp}{2\Delta}, \tag{4}$$

for opening mode and

$$\frac{\partial w(t)}{\partial X_1}=-\frac{\upsilon B}{2E}\left[\sum_{N=1}^{\infty} D_N(t)\left(\frac{N}{2}-1\right) r^{\left(\frac{N}{2}-2\right)}\sin\left[\left(\frac{N}{2}-2\right)\theta\right]\right] =\frac{Mp}{2\Delta}, \tag{5}$$

$$\frac{\partial w(t)}{\partial X_2}=-\frac{\upsilon B}{2E}\left[\sum_{N=1}^{\infty} D_N(t)\left(\frac{N}{2}-1\right) r^{\left(\frac{N}{2}-2\right)}\cos\left[\left(\frac{N}{2}-2\right)\theta\right]\right] =\frac{Mp}{2\Delta}, \tag{6}$$

for in-plane shear mode. In the above (r, θ) are polar coordinates centered at the crack tip. In equations (3)–(6), C_N and D_N are coefficients for mode-I and mode-II, respectively. The above equations can be used for a dynamically loaded stationary crack by making an implicit assumption that inertial effects enter the coefficients while retaining the functional form of the quasi-static counterpart. Accordingly, the coefficients C_N and D_N are represented as functions of time t.

Pre-Crack Initiation Period

Fig. 6(a) and (b) show the crack tip coordinate systems followed in this work for digitizing CGS fringes and to extract mode-I and mode-II stress intensity factors. Consider the situation prior to crack initiation as shown in Fig. 6(a). Here X_1-X_2 is the global co-

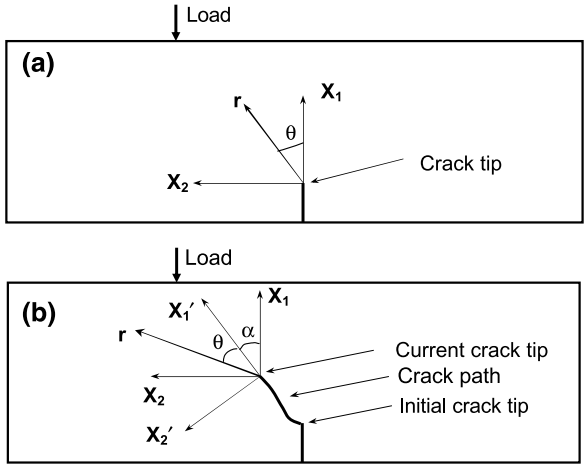

Fig. 6. Global and local crack tip coordinate systems for (**a**) stationary crack and (**b**) propagating crack

ordinate system which is aligned with the local (crack tip) coordinate system. Since the crack is aligned with the principal direction of the gratings, CGS governing equation for mixed-mode stress intensity factors is obtained by superposing mode-I and mode-II fields from equations (3) and (5):

$$\frac{\partial w(t)}{\partial X_1} = \frac{\upsilon B}{2E}\left[\begin{Bmatrix}\sum_{N+1}^{\infty} C_N(t)\left(\frac{N}{2}-1\right)r^{\left(\frac{N}{2}-2\right)}\cos\left[\left(\frac{N}{2}-2\right)\theta\right]\end{Bmatrix}+\begin{Bmatrix}\sum_{N=1}^{\infty} D_N(t)\left(\frac{N}{2}-1\right)\mathrm{r}^{\left(\frac{N}{2}-2\right)}\sin\left[\left(\frac{N}{2}-2\right)\theta\right]\end{Bmatrix}\right] = \frac{Mp}{2\ \Delta} \tag{7}$$

The coefficients of first terms ($N = 1$) in the asymptotic series are related to mode-I and mode-II stress intensity factors $K_{ID}(t)$ and $K_{IID}(t)$, respectively, as

$$C_1(t) = K_{ID}(t)\sqrt{\frac{2}{\pi}}, D_1(t) = K_{IID}(t)\sqrt{\frac{2}{\pi}}. \tag{8}$$

Post-Crack Initiation Period

Since the crack path during growth can be along an arbitrary direction, it is convenient to define a local (variable) coordinate system (X_1', X_2') which is instantaneously aligned with the current crack path as shown in Fig. 6(b). While digitizing fringes in the post-crack initiation period, coordinates of the digitized points are transformed from global system (X_1-X_2) to the local rotated system (X_1', X_2'). CGS fringes represent surface slopes as indicated by equation (2). Since the crack is at an arbitrary angle, surface slope has to be resolved along the local coordinates as,

$$\frac{\partial w}{\partial X_1} = \frac{\partial w}{\partial X_1'}\cos\alpha + \frac{\partial w}{\partial X_2'}\sin\alpha, \tag{9}$$

where α is the crack kink angle as shown in Fig. 6(b). By using modified versions of equations (3)–(6) and (9), for a steadily propagating crack, deformations can be related to optical measurements as,

$$-\frac{\upsilon B}{2E}\left[\begin{Bmatrix}-\frac{1}{2}r_l^{-3/2}\begin{Bmatrix}f(V;C_L,C_S)C_1(t)\cos\left(\frac{3\theta_l}{2}+\alpha\right)+\\ g(V;C_L,C_S)D_1(t)\sin\left(\alpha-\frac{3\theta_l}{2}\right)\end{Bmatrix}+\\ \sum_{N=2}^{\infty} C_N(t)\left(\frac{N}{2}-1\right)r_l^{\left(\frac{N}{2}-2\right)}\cos\left\{\alpha+\left(2-\frac{N}{2}\right)\theta_l\right\}+\\ \sum_{N=2}^{\infty} D_N(t)\left(\frac{N}{2}-1\right)r_l^{\left(\frac{N}{2}-2\right)}\sin\left\{\alpha+\left(\frac{N}{2}-2\right)\theta_l\right\}\end{Bmatrix}\right] = \frac{Mp}{2\Delta}. \tag{10}$$

Where f and g denote functions associated with instantaneous crack velocity, and (r_l, θ_l) denote crack tip polar coordinates associated with a growing crack,

$$r_l = \left\{\left(X_1'\right)^2 + \alpha_L^2\left(X_2'\right)^2\right\}^{1/2}, \quad \theta_l = \tan^{-1}\left(\frac{\alpha_L X_2'}{X_1'}\right).$$

For plane stress, the functions f and g are given by [6],

$$f(V;C_L,C_S) = \left(\frac{1+\nu}{1-\nu}\right)\frac{\left(1+\alpha_S^2\right)\left(1-\alpha_L^2\right)}{4\alpha_L\alpha_S-\left(1+\alpha_S^2\right)^2}, \tag{11}$$

$$g(V;C_L,C_S) = \left(\frac{1+\nu}{1-\nu}\right)\frac{2\alpha_S\left(1-\alpha_L^2\right)}{4\alpha_L\alpha_S-\left(1+\alpha_S^2\right)^2}, \tag{12}$$

where $\alpha_L = \left[1-\frac{\rho(1-\nu)}{2\mu}V^2\right]^{1/2}$ and $\alpha_S = \left[1-\frac{\rho}{\mu}V^2\right]^{1/2}$. Here V is the crack speed, μ and ρ are *local* shear modulus and mass density, respectively.

Analyzing of fringes in FGM using equations (7) and (10) implicitly assumes a locally homogeneous material behavior in the crack tip vicinity. This needs

justification since crack tip stress fields for steadily and transiently growing cracks for nonhomogeneous material have been made available by Shukla and coworkers [5, 6] in recent years. For a relatively shallow elastic gradients such as the ones used in the current study, it is shown in an earlier work [9] that results would not be greatly affected (differences being less than 5%) by such an assumption. Further, there are also difficulties associated with utilizing existing FGM crack tip fields [5] to analyze optical interferograms in the current work. Specifically, theoretical derivations [5,6] use spatial variation of elastic modulus and mass density to have a single nonhomogeneity parameter for an exponential type description or assume a constant mass density. However, particulate composites in general and glass-filled epoxy FGM prepared for this work in particular have significantly different elastic modulus and mass density variations (2.5 fold (4.0 GPa to 10 GPa) over a width of 43mm where as mass density variation was 1.5 fold (1175 kg/m3 to 1700 kg/m3) over the same length) which limit the usage of those reported equations.

The role of crack tip transients namely rate of change of SIF and crack accelerations/decelerations are described in Ref. [6]. Based on the experimental results (to be described later), these effects were found to be negligible for the current work. For example, it is noted in Ref. [6] that the rate of change of SIF on out-of-plane displacements becomes relatively insignificant if $dK_{ID}(t)/dt$ is within 1.0×10^5 MPa $m^{1/2}$/sec and in the current work $dK_{ID}(t)/dt$ values were an order of magnitude less than this value. Also out-of-plane displacements are said to be minimally affected if accelerations are less than 1.0×10^7 m/sec^2. Again, maximum acceleration recorded during this work was an order of magnitude lower. Thus extracting SIF from fringes using steady-state assumptions is quite reasonable.

While digitizing interferograms, the current crack tip location was first identified and the crack kink angle was evaluated. Simultaneously, around the crack tip, the fringe location (r, θ) and the fringe order M were also recorded. An over-deterministic least-squares analysis [23, 25] was performed on the collected data to extract SIFs. To maintain the accuracy of the digitized data points as well as to exclude the region where 3D-effects [23] dominate, data points in the range ($0.3 < r/B < 1.3$) behind the crack tip were chosen for analysis. The crack speed history was also determined by differentiating crack length history with respect to time. That is, for every 5 μs after crack initiation, horizontal and vertical components of crack increment were identified and resultant crack increment was calculated. These were sequentially added to get the instantaneous absolute crack length. The crack speed history was estimated as

$$v_i = \left(\frac{da}{dt}\right)_i = \frac{a_{i+1} - a_{i-1}}{t_{i+1} - t_{i-1}} \tag{13}$$

where $a_i = a_{i-1} + \Delta a$ and $\Delta a = \sqrt{(\Delta a_h)^2 + (\Delta a_v)^2}$. Here Δa_h and Δa_v are horizontal and vertical components of the crack increment, respectively.

Results

Experimental Details

Mixed-mode fracture experiments conducted on FGM samples included two types: (a) A crack on the compliant side of the sample with impact occurring on the stiffer side and (b) A crack on the stiffer side of the sample with impact occurring on the compliant side. A homogeneous sample having the same geometry and made out of Plexiglas was also tested under similar experimental conditions for comparative purposes. The two configurations of FGM and the homogeneous sample used in experiments are shown schematically in Fig. 7(a)–(c) as insets. Here, the elastic modulus at the edge of the cracked sheet behind the crack tip is denoted as E_1 and the one ahead of the crack tip as E_2. With this notation, type-(a) experiments correspond to $E_1 < E_2$ and type-(b) experiments correspond to $E_1 > E_2$. Except for this change all other conditions are same for type-(a) and (b) experiments. Specimens were subjected to mixed-mode loading by impacting at an offset distance (S = 25.4 mm) relative to the initial crack plane. Since specimen dimensions and all other experimental conditions are same, any difference in stress intensity factor histories, crack speed histories, and crack path are directly attributable to the compositional gradients (elastic as well as fracture toughness gradients).

Representative fringes are shown in Fig. 7 for experiments conducted on two types of FGM samples as well as a homogeneous[1] sample. In all the Fig. 8(a)–(c), the first two interferograms correspond to pre-initiation period, third image at a time instant when

[1] FGM samples being particulate polymer composites whereas homogeneous sample is made of an amorphous polymer (Plexiglas), emphasis is placed on macroscopic fracture behaviors (crack path and mode-mixity history) rather than absolute values of fracture parameters (crack initiation time, SIFs corresponding to crack initiation and growth).

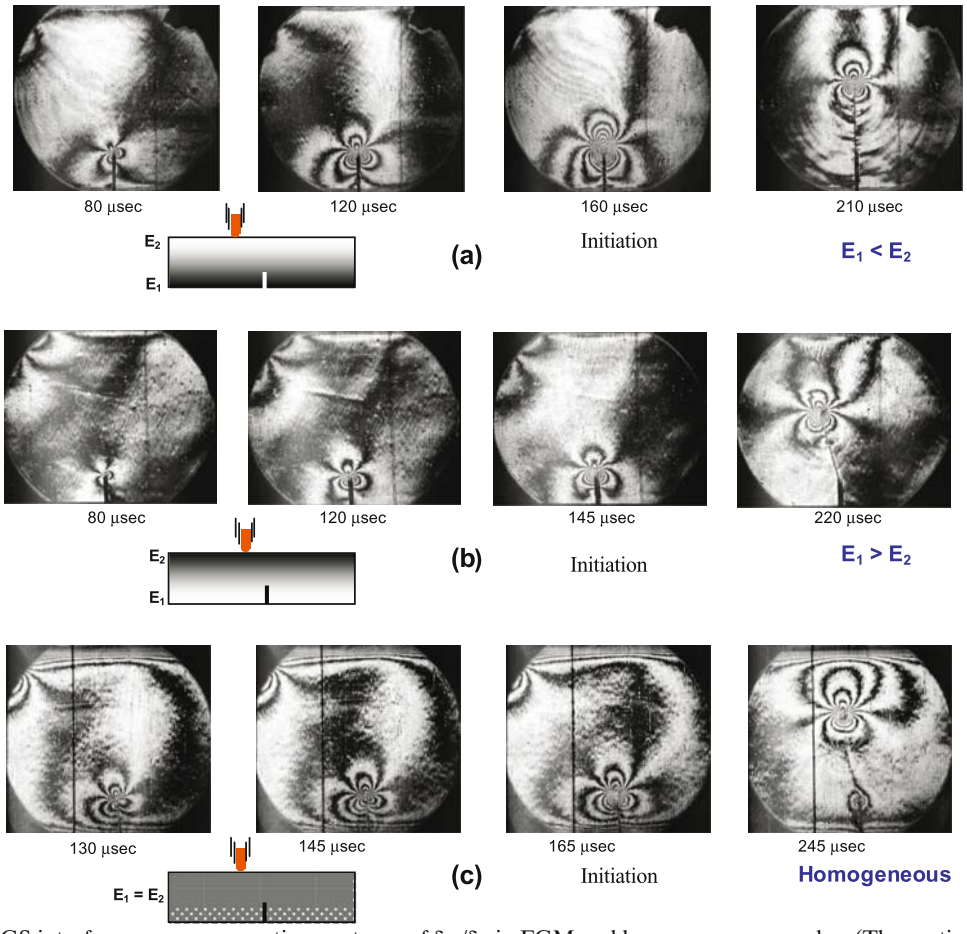

Fig. 7. Selected CGS interferograms representing contours of δw/δx in FGM and homogeneous samples. (The vertical line is at 10 mm from the crack). (**a**) crack on the compliant side and (**b**) crack on the stiffer side (**c**) homogeneous (Plexiglas) sample

the crack was about to initiate and the fourth one is in the post-initiation period. The legends correspond to the time instant at which the image was recorded after impact. The impact point was located outside the window of observation and hence cannot be seen in these images. Once the impact occurs, compressive stress waves originate at the impact point and travel through the specimen. They reflect from the bottom edge and sides of the sample as tensile waves and load the crack tip. At about 60 µs after impact, crack tip

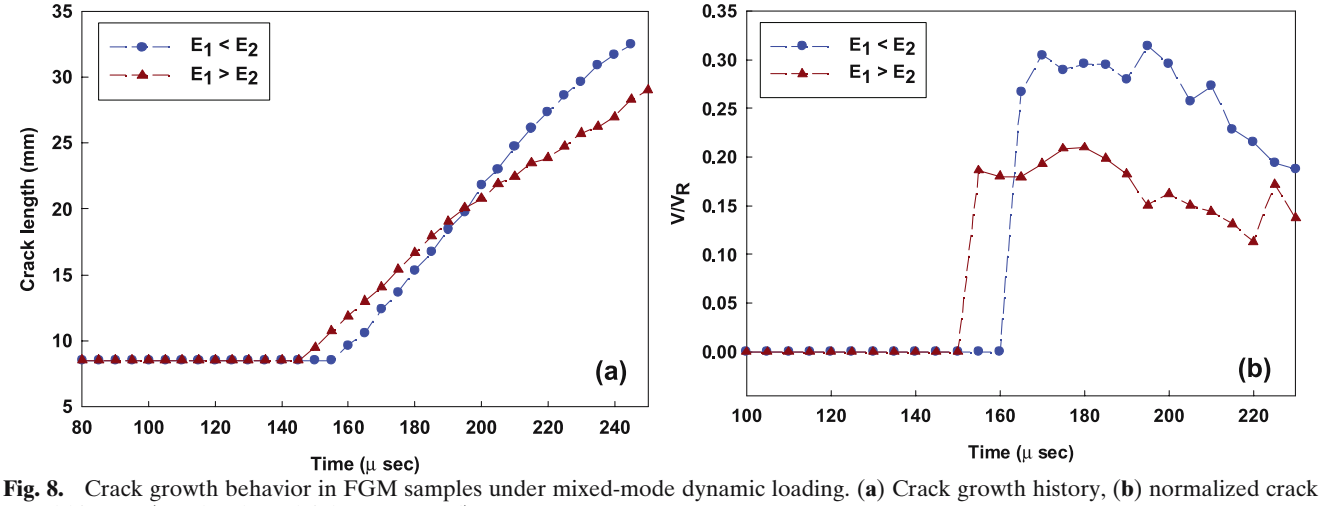

Fig. 8. Crack growth behavior in FGM samples under mixed-mode dynamic loading. (**a**) Crack growth history, (**b**) normalized crack speed history. (V_R: local Rayleigh wave speed)

experiences stresses large enough to exhibit fringes after which a monotonic increase in the number of fringes around the crack tip was seen. Two important observations can be made from these images. Firstly, more number of fringes are seen for the case $E_1 < E_2$ compared to $E_1 > E_2$ indicating more deformation around the crack tip when the crack is located on the compliant side. On the other hand, fewer fringes around the crack tip are seen when it is situated on the stiffer side. Secondly, the crack tip loading is essentially of mixed-mode type. That is, one can see clearly tilting of fringe lobes towards the left of the initial crack indicating the presence of negative shear component in the beginning. However, just before crack initiation, fringes tend to become relatively symmetric with respect to the crack suggesting predominantly mode-I deformation and possibly vanishing K_{II} at initiation.

Crack Growth and Crack Speed Histories

A number of experiments (typically three) were conducted for both the configurations $E_1 < E_2$ and $E_1 > E_2$ to ensure repeatability. In the following, results are presented for a representative experiment of each configuration. Fig. 8(a) shows crack growth histories for both the experiments. The crack initiates at about 145 μ sec when it is situated on the stiffer side and at about 160 μ sec when it is located on the compliant side. This is in commensurate with the fact that more crack tip deformation occurs for the case $E_1 < E_2$ than $E_1 > E_2$ as evidenced by a relatively large number of fringes in Fig. 7(a) than in Fig. 7(b). Also, the slope of the crack growth history curve is steeper for $E_1 < E_2$ indicating an overall higher crack speed in this case.

The crack speed histories were computed from crack growth histories and are shown in Fig. 8(b). Here, the crack speeds are normalized using local Raleigh wave speed (V_R). Crack speed histories indicate that the crack accelerates following initiation to a maximum value with a subsequent oscillatory behavior as the crack is driven forward by discrete wave reflections from the boundaries of the specimen. Sudden acceleration after initiation is attributed to the finite root radius (150 μm) of the initial crack inserted into the samples. The data suggests that the average crack speeds are approximately 310 m/sec (0.3 V_R) for $E_1 < E_2$ and 250 m/sec (0.2 V_R) for $E_1 > E_2$. This shows that crack speeds are generally higher when the crack is located on the compliant side of the sample. Once the crack initiates, the normalized crack speed remains nearly constant until crack propagates through the lower half the specimen. Subsequently, crack speed shows a decreasing trend for both the configurations as the crack tip approaches the impact point.

Mixed-Mode Stress Intensity Factor Histories

The stress intensity factors for both the cases were extracted as explained previously and are shown in Fig. 9. In this plot, the crack initiation time is taken as ($t = 0 \rightarrow t_i$) so that positive values correspond to post-initiation period and negative ones to the pre-initiation period. Stress intensity factors were initially computed by considering K-dominant term ($N = 1$ in equation (7)) and up to 4 higher order terms ($N = 6$) sequentially. After analyzing a few experiments, it was found that the K-dominant solution ($N = 1$) was inadequate to capture mixed-mode stress intensity factor histories throughout the experiment. A Two-term ($N = 3$ in equation (7)) or a Three-term ($N = 4$)

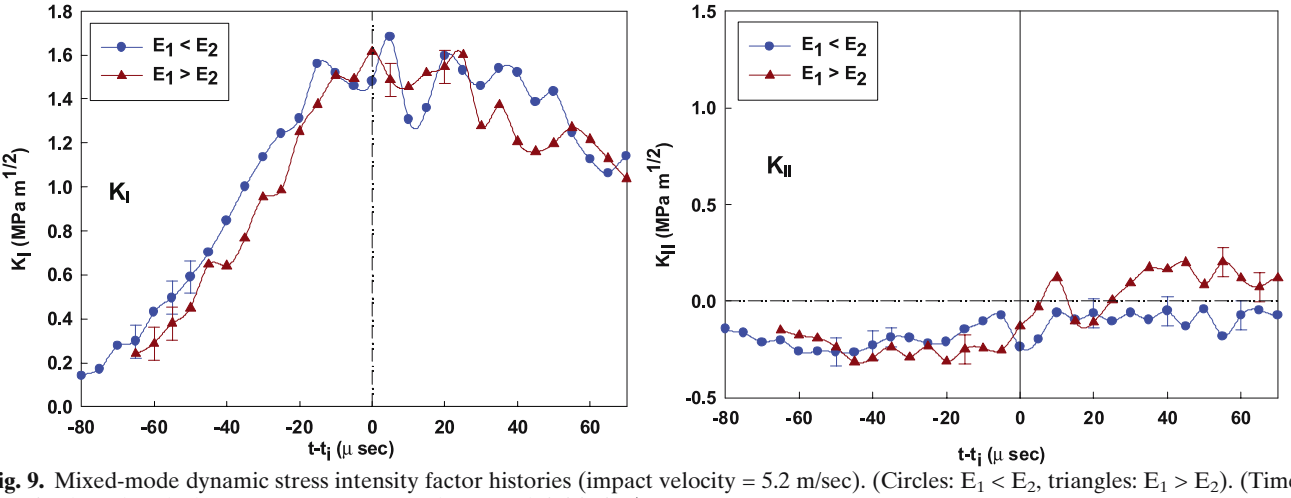

Fig. 9. Mixed-mode dynamic stress intensity factor histories (impact velocity = 5.2 m/sec). (Circles: $E_1 < E_2$, triangles: $E_1 > E_2$). (Time base is altered such that $t - t_i = 0$ corresponds to crack initiation)

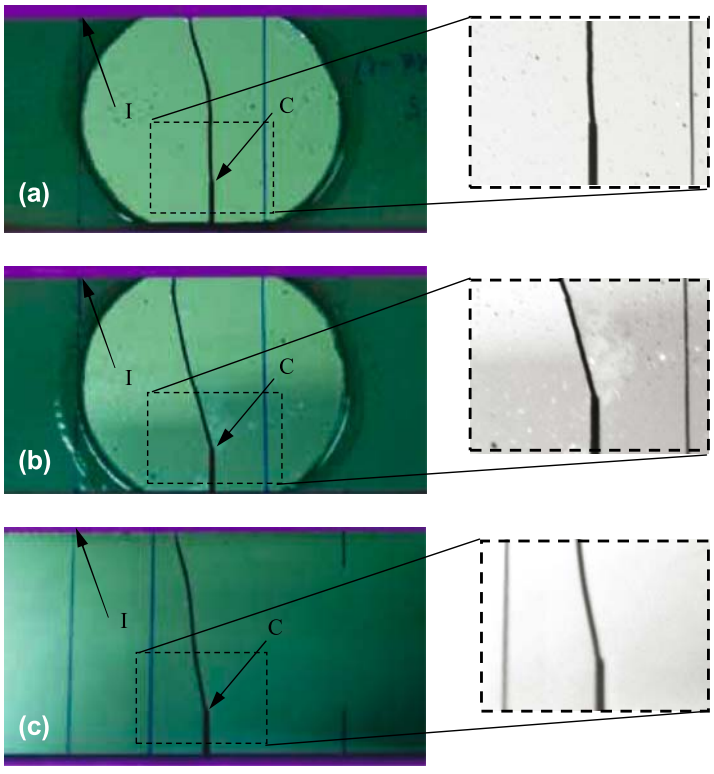

Fig. 10. Photographs showing fractured specimens for (**a**) FGM with a crack on the compliant side ($E_1 < E_2$), (**b**) FGM with a crack on the stiffer side ($E_1 > E_2$) and (**c**) a homogeneous specimen. Impact point is indicated by letter "I" and initial crack tip by letter "C"

solution was found to be stable and capture the overall fracture behavior.

In Fig. 9(a) mode-I stress intensity factor monotonically increases up to crack initiation. The rate of increase of in the stress intensity factor in the early stages of crack tip loading is about 3×10^4 MPa $m^{1/2}$/s. Following crack initiation, a small dip in K_I is seen suggesting sudden release of stored energy from the initial notch tip. After this drop, K_I values show a modest increase in the case of $E_1 < E_2$ since the crack is running into a gradually reinforced region with higher volume fraction of the filler. However, for the case of $E_1 > E_2$, after initiation K_I gradually decreases in the observation window. The mode-II SIFs (Fig. 9(b)) for both FGM are initially negative and once initiation occurs, K_{II} continues to be at a small but negative value for $E_1 < E_2$ whereas it attains a small but positive value for $E_1 > E_2$ within the observation window.

Figure 10 shows photographs of the fractured specimens. The impact point is located on the top edge of each image and the initial crack tip is at the bottom edge as indicated. The reflective area on each specimen surface is the region of interest where the surface deformations are monitored. A vertical line (on right side of the crack for FGM samples and on left side of the crack for homogeneous sample) seen in these figures is located 10 mm away from the crack tip which helps to establish the scale. In Fig. 10(a), the crack is situated on the compliant side ($E_1 < E_2$). Figure 10(b) corresponds to the opposite configuration ($E_1 > E_2$) and in Fig. 10(c), fractured Plexiglas specimen is shown. The striking feature between these images is the differences in crack paths in the lower half of the specimen. For the case $E_1 < E_2$, the crack initiation occurs almost like a mode-I crack with an *initial* kink angle of ~4° with respect to the X_1-axis whereas for the case $E_1 > E_2$, crack growth occurs at an *initial* kink angle of $\alpha \sim 16°$, (see Fig. 10(b)). Subsequent crack growth (say, 4 mm beyond the initial growth) in case of $E_1 < E_2$ shows a tendency for the crack to grow nearly along the X_1-direction. On the other hand, in case of $E_1 > E_2$ crack growth is essentially self-similar with continued growth at an angle of ~16° with respect to the X_1-axis. In the upper half of the sample, the crack growth is affected by a combination of free-edge and impact point effects. All the parameters (specimen dimensions, impact velocity, etc.) are same for these two experiments except the reversal of compositional grading. Hence, the differences in the crack paths are attributable directly to the combined effects of elastic gradients as well as fracture toughness gradients. Having seen distinctly different crack paths for the above two configurations, homogeneous specimens made out of Plexiglas were also tested under similar conditions and the resulting crack path is shown in Fig. 10(c). The crack shows an initial kink angle $\alpha \sim 10°$

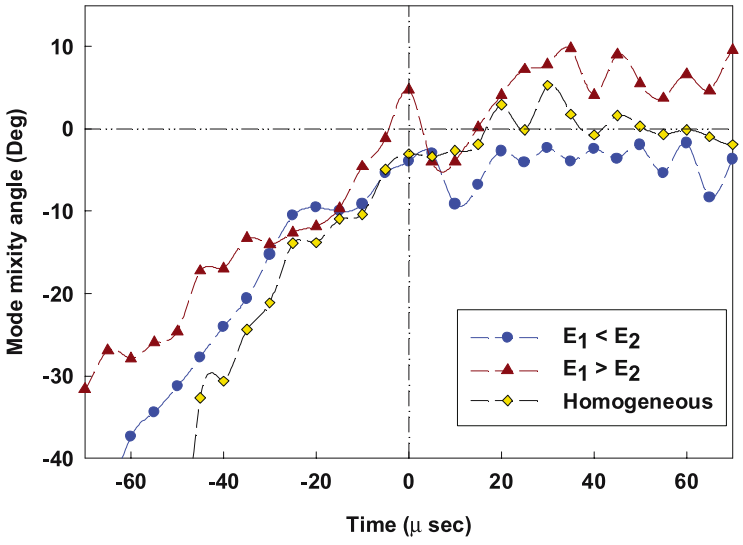

Fig. 11. Mode mixity histories for FGM and homogeneous samples. Crack initiation is indicated by a vertical line at $(t - t_i) = 0$, (t_i = time of crack initiation in μ sec)

which is bounded by the ones for the two FGM configurations.

The relative amount of in-plane shear stress to normal stress near the crack tip can be quantified by mode mixity $\psi = \tan^{-1}(K_{II}/K_I)$. The mode mixity histories for all the three cases are plotted in Fig. 11. A large negative value of ψ can be seen at initial stages after impact indicating the presence of significant negative in-plane shear component at the crack tip. But just before crack initiation, ψ approaches zero. This suggests that crack initiation occurs under dominant mode-I conditions in all the three cases. Once the crack initiates, ψ remains slightly negative for the case $E_1 < E_2$ and is slightly positive for $E_1 > E_2$ as shown in the Fig. 11. Interestingly for the homogeneous sample, mode mixity is essentially zero during crack propagation suggesting the possibility of crack growth in FGM occurring under conditions of nonzero K_{II}.

Initial Crack Path Prediction

Maximum tangential stress (MTS) criteria introduced by Erdogan and Sih [26] is found to predict small crack kink angles in FGM reasonably well under static loading conditions for glass-filled epoxy [19] and hence its validity in the current dynamic experiments is considered next. The MTS criteria states that the crack will kink along the direction in which the tangential stress is maximum. That is, the crack kink angle α can be computed uniquely by solving the equation,

$$K_{\mathrm{I}} \sin\alpha + K_{\mathrm{II}}(3\cos\alpha - 1) = 0. \tag{14}$$

where K_{I} and K_{II} are mode-I and mode-II stress intensity factors. The kink angle α is measured positive in counter-clockwise direction in usual crack tip coordinate system (see Fig 5(b)).

In this work, crack kink angles at initiation are predicted based on SIF histories 10 μ sec (2 frames) prior to crack initiation. The kink angles thus predicted are verified by the observed angles close to the initial crack tip. The crack kink angle in experiments was determined from interferograms using MATLAB™ as follows. The images corresponding to post-crack initiation regime were loaded into the software environment. First, a point corresponding to the current crack tip was located. Then, a second point was located on the crack establishing a tangent to the current crack path. By using

Table 2(a) Predicted crack kink angle based on estimated SIF data from three CGS interferograms before crack initiation

$E_1 < E_2$		$E_1 > E_2$	
Time (μs)	α	Time (μs)	α
150	7.9°	135	17.6°
155	5.8°	140	18.3°
Average	**6.8°**		**17.9°**

Table 2(b) Observed crack kink angle from three CGS interferograms just after crack initiation

$E_1 < E_2$		$E_1 > E_2$	
Time (μs)	α	Time (μs)	α
165	4.3°	150	16.8°
170	5.0°	155	16.4°
Average	**4.6°**		**16.6°**

these two points, horizontal and vertical components of crack extension were identified and the crack kink angle was calculated. A third point was marked on the initial crack tip to continuously track the current crack tip with respect to the initial crack tip. The crack kink angle thus calculated was also verified by post-mortem examination of the fractured specimens.

Table 2(a) lists crack kink angles predicted by MTS criteria using estimated SIFs from two interferograms prior to crack initiation. The crack initiation time is ~160 μs for $E_1 < E_2$ and ~145 μs for $E_1 > E_2$. It can be seen from Table 2(a) that the average value of the angle α is greater for $E_1 > E_2$ compared to $E_1 < E_2$ by about 11 degrees. This indicates that crack would kink more when it is situated on the stiffer side compared to the compliant side of the FGM. This can be readily verified from Fig. 10. Crack propagation in fractured specimens showing initial 10 mm of crack growth are shown as insets in Fig. 11(a) and (b) for $E_1 < E_2$ and $E_1 > E_2$, respectively. The observed kink angles are listed in Table 2(b) for 5 and 10 μs after crack initiation. It can be seen from these two tables that average values of crack kink angle predicted by MTS criteria agree reasonably well with the observed ones at early stages of crack growth.

Conclusions

Mixed-mode dynamic fracture experiments were conducted on FGM under low-velocity impact loading conditions. Transient crack tip deformations were mapped for pre- and post-crack initiation periods. Two configurations namely a crack on the compliant side ($E_1 < E_2$) and a crack on the stiffer side ($E_1 > E_2$) of the specimen were investigated. An experiment was also conducted on a homogeneous sample under similar conditions. Following conclusions were drawn from the study:

- Crack initiates earlier for the case $E_1 > E_2$ compared to $E_1 < E_2$. Higher crack speed was observed in the latter case compared to the former.
- Crack initiation in both the FGM configurations occurred when K_{II} values approached zero. Yet, during crack growth K_{II} remained at a small negative value when the crack was on the compliant side but maintained a small positive value when it was on the stiffer side of the FGM sheet. This raises the possibility of a non-zero K_{II} during mixed-mode dynamic crack growth in FGM.
- The crack paths differed significantly for the two FGM configurations studied. That is, the crack kinked less when situated on the compliant side compared to the stiffer side of the FGM sample. The differences in crack paths are attributed to a combination of elastic and fracture toughness gradients.
- The initial crack kink angle was predicted for both the configurations using MTS criteria based on the SIF values just prior to crack initiation. Thus predicted crack kink angles agree reasonably well with the observed ones during early stages of the crack growth.

Acknowledgments Authors would like to thank U. S. Army Research Office for supporting this research through grant W911NF-04-1-0257 (Dr. Bruce LaMattina, Program Manager).

References

1. Delale F, Erdogan F (1983) The crack problem for a non-homogeneous plane. ASME J Appl Mech 50:609–614.
2. Eischen JW (1987) Fracture of non-homogeneous materials. Int J Fract 34:3–22.
3. Jin ZH, Batra RC (1996) Some basic fracture mechanics concepts in functionally graded materials. J Mech Phys Solids 44(8):1221–1235.
4. Gu P, Asaro RJ (1997) Cracks in functionally graded materials. Int J Solids Struct 34(1):1–17.
5. Parameswaran V, Shukla A (1999) Crack tip stress fields for dynamic fracture in functionally graded materials. Mech Mater 31:579–596.
6. Chalivendra V, Shukla A (2005) Transient elastodynamic crack growth in functionally graded materials. J Appl Mech 72:237–248.
7. Rousseau CE, Tippur HV (2001) Influence of elastic gradient profiles on dynamically loaded functionally graded materials: cracks along the gradient. Int J Solids Struct 38:7839–7856.
8. Rousseau CE, Tippur HV (2002) Evaluation of crack tip fields and stress intensity factors in functionally graded elastic materials: cracks parallel to elastic gradient. Int J Fract 114:87–111.
9. Rousseau CE, Tippur HV (2001) Dynamic fracture of compositionally graded materials with cracks along the elastic gradient experiments and analysis. Mech Mater 33:403–421.
10. Kirugulige MS, Kitey R, Tippur HV (2004) Dynamic fracture behavior of model sandwich structures with functionally graded core; a feasibility study. Compos Sci Technol 65:1052–1068.
11. Wang W, Nakamura T (2004) Simulations of crack propagation in elastic–plastic graded materials. Mech Mater 36:601–622.
12. Kim JH, Paulino GH (2004) Simulation of crack propagation in functionally graded materials under mixed mode and non-proportional loading. Int J Mech Mater Des 1:63–94.
13. Ramaswamy S, Tippur HV, Xu L (1993) Mixed mode crack tip deformations studied using a modified flexural specimen and Coherent Gradient Sensing. Exp Mech 33:218–227.
14. Lee H, Krishnaswamy S (2000) Quasi-static propagation of sub interfacial cracks. ASME J Appl Mech 67: 444–452.
15. Mason JJ, Lambros J, Rosakis AJ (1992) The use of a coherent gradient sensor in dynamic mixed-mode fracture mechanics experiments. J Mech Phys Solids 40(3): 641–661.
16. Prabhu S, Lambros J (2000) A combination optical method of lateral shearing interferometry and Caustics. Exp Mech 40(4):376–383.
17. Madhusudhana KS, Narasimhan R (2002) Experimental and numerical investigations of mixed-mode crack growth resistance of a ductile adhesive joint. Eng Fract Mech 69:865–883.
18. Butcher RJ, Rousseau CE, Tippur HV (1998) A functionally

graded particulate composite: preparation, measurements and failure analysis. Acta Mater 47(1):259–268.
19. Rousseau CE, Tippur HV (2000) Compositionally graded materials with cracks normal to the elastic gradient. Acta Mater 48:4021–4033.
20. Marur PR, Tippur HV (2000) Dynamic response of bi-material and graded interface cracks under impact loading. Int J Fract 114:87–111.
21. Dally JW, Sanford RJ (1987) Strain gage methods for measuring the opening mode stress intensity factor, K_I. Exp Mech 49:381–388.
22. Maleski MJ, Kirugulige MS, Tippur HV (2004) A method for measuring mode-I crack tip constraint under static and dynamic loading conditions. Exp Mech 44(5):522–532.
23. Tippur HV, Krishnaswamy S, Rosakis AJ (1991) Optical mapping of crack tip deformations using the methods of transmission and reflection Coherent Gradient Sensing: a study of crack tip K-dominance. Int J Fract 52:91–117.
24. Williams ML (1959). J Appl Mech 24:109–114.
25. Sanford RJ (1989) Determining fracture parameters with full-field optical methods. Exp Mech 29:241–247.
26. Erdogan F, Sih GC (1963) On the crack extension in plates under plane loading and transverse shear. J Basic Eng-Trans ASME 85D(4):519–525.